minerals

MDPI

Article

Late Cretaceous-Paleocene Arc and Back-Arc System in the Neotethys Ocean, Zagros Suture Zone

Yousif Mohammad [1,*], Kurda Abdulla [1] and Hossein Azizi [2]

[1] Department of Geology, College of Science, University of Sulaimani, Sulaymaniyah 46011, Iraq; kurda.abdulla@univsul.edu.iq
[2] Department of Mining Engineering, Faculty of Engineering, University of Kurdistan, Sanandaj 66177-15175, Iran; h.azizi@uok.ac.ir
* Correspondence: yousif.mohammad@univsul.edu.iq; Tel.: +964-7724499001

Abstract: The Bulfat Igneous Complex comprises the Bulfat and Walash groups and is situated in the Zagros Suture Zone, in the junction of Arabian and Eurasian plates. Zircon U-Pb data indicate an age of 63.7 ± 1.5 Ma for the trondhjemite rocks within the Bulfat group. Walash group is primarily composed of basalt to andesite rocks, interbedded with sedimentary rocks. Zircon U-Pb dating yields an age of 69.7 ± 2.7 Ma for the Walash group. Whole rocks chemistry shows that the Bulfat rocks have affinity to MORB and calc alkaline series but Walsh are mainly plot in the calc alkaline field. Whole rocks Sr-Nd isotope ratios show that the ^{143}Nd/^{144}Nd (i) changes from 0.51243 to 0.52189 and 87Sr/86Sr(i) ratios vary from 0.70345 to 0.7086. The calculated εNd(t) values, based on the CHUR, yield predominantly high positive values ranging from +6 to +8 for most samples. However, a few samples exhibit lower values (+2 to +3). Our data suggest that the interaction between lithospheric (depleted mantle, MORB-Like) and asthenospheric mantle (OIB-like) melts significantly controlled the magmatic evolution of the Bulfat group. The strong positive εNd(t) values (ranging from +6 to +8) align more consistently with a highly depleted lithospheric mantle source for the Walsh group. Therefore, the gradual transition from an arc signature at 70 Ma to a MORB signature around 63 Ma, occurred over a relatively short period of about 10 million years, and indicates the presence of an arc and back-arc system in the Neotethys ocean before the collision of the Arabian and Iran plates during the Cenozoic.

Keywords: island arc; Zagros Sutures Zone; oceanic arc-back-arc system; collision zone; Iraq

check for updates

Citation: Mohammad, Y.; Abdulla, K.; Azizi, H. Late Cretaceous-Paleocene Arc and Back-Arc System in the Neotethys Ocean, Zagros Suture Zone. *Minerals* **2023**, *13*, 1367. https://doi.org/10.3390/min13111367

Academic Editors: Fuhao Xiong, Bin Liu and Petrus J Le Roux

Received: 30 September 2023
Revised: 14 October 2023
Accepted: 21 October 2023
Published: 26 October 2023

1. Introduction

In the northeast of Iraq along the collision zone, a liner scattered bodies of ultramafic and mafic rocks combined with deep marine and pelagic sedimentary rocks has been identified. These rocks are believed to represent remnants of the Neotethys ocean crust, which underwent obduction during the collision between the Arabian and Iran (Eurasia) plates in the Cenozoic [1]. These suites are recognized in different parts of the region: the Penjween and Mawat Ophiolite Complexes in the south [2–5], Bulfat Igneous Complex in the central part [6–12], and Hasanbag Ophiolite Complex in the north [13]. The Penjween and Mawat Ophiolite Complexes are primarily dominated by depleted mantle peridotites and gabbroic rocks, accompanied by some of felsic rocks. However, the volcanic components of these complexes remain yet to be identified. On the other hand, the Bulfat Igneous Complex is mainly composed of marginal basaltic rocks surrounding the predominant gabbroic rocks, while ultramafic rocks are concentrated at the central region. Meanwhile, the Hasanbag Complex is predominantly comprised of volcanic rocks, with the absence of ultramafic and gabbroic rocks.

The many hypotheses regarding the origin of igneous rocks in the Kurdistan Region in the north east of Iraq can be attributed to two main factors. Firstly, the absence of comprehensive and up-to-date regional geologic maps that accurately portray the igneous rock-dominated terrain has led to uncertainties. Secondly, the conclusions drawn from many studies on the igneous rock along northeastern Iraq are primarily grounded in geochemical analyses. Consequently, due to these limitations, many ideas have been proposed regarding the genesis of these rocks. These hypotheses encompass concepts such as the existence of oceanic ophiolites [1,4,7,14], and plume-type magmatism within the passive margins of nascent oceanic crusts [15].

The Bulfat Igneous Complex has attracted the interest of geologists and the different parts of the complex have been studied extensively [6–13,16–20]. The presence of intraoceanic arcs within the Neotethys Ocean during the Eocene, as indicated by the Walash and Bulfat groups in Iraq, prior to the collision of the Arabian and Iranian continental plates, remains a topic of ongoing discussion. The proposed age of the Bulfat Igneous complex was dated 34.78 Ma, as determined by the ^{39}Ar-^{40}Ar dating technique [18]. Similarly, Ali [7] utilized the U-Pb dating of one zircon grain method and suggested an age of about 39.0 ± 0.5 Ma for the same igneous complex. Nutman et al. [19] inferred that the 48 Ma old granite within the Bulfat Igneous complex originated from the partial melting of previously recycled mafic crust. Also, Elias et al. [21] provided evidence indicating of an intrusion within the Bulfat Igneous complex prior to the 50 Ma. Indeed, Koshnaw et al. [22] based on extensive detrital zircon (DZ) study, indirectly postulated that the proto Walash group originated as a back-arc to arc system during the late Cretaceous to Paleocene. In consideration of these findings, an improved understanding of the origins of the Bulfat and Walash groups on the Iraqi side of the Zagros orogenic belt will play a significant role in resolving this geologic puzzle.

In this research, we present for the first time some new U-Pb zircon age dates, whole-rock chemistry, and Sr–Nd isotope ratios of both mafic and felsic rocks of the Bulfat and Walash groups. These insights are further enriched with a new geologic mapping and fieldwork. Finally, we introduce a novel geodynamic model that illustrates occurrences of intraoceanic arc during the Late Cretaceous-Paleocene, followed by continental collisions in the Eocene.

2. Background and Field Observations

The Bulfat Igneous Complex, in the northern part of Sulaymaniyah city, has a distinctive lozenge shape and is positioned between the Sanandaj-Sirjan Zone (SaSZ) to the east and the Walash volcanic rocks to the west (Figures 1 and 2). This complex comprises many rock types, including red pelagic sediments, a basalt layer, substantial foliated gabbroic and dioritic rocks with some tectonite peridotite.

Additionally, notable high-grade metamorphic rocks, such as migmatite with exposed stripped gneiss structures and a mylonitic texture, are exposed in the Qandol area. These high-grade metamorphic rocks are located both at the uppermost part of the Bulfat Igneous Complex, adjacent to the Zagros Suture Zone, and at the lowermost section, in proximity to the mantle peridotite layer.

The Bulfat Igneous Complex is confined or situated between two prominent fault systems, which essentially envelop it. As a result, ongoing fault-related activities manifest through pronounced dynamic deformations, the presence of cataclasites, and the development of mylonite textures. This situation categorizes the Bulfat Complex as an archetypal representation of a shear zone, positioned between the Zagros Main fault system in the east and the Qaladiza-Qandol fault system in the west (Figure 2).

Most parts of the complex have been influenced by a variable degree of dynamic deformation, rendering the visual identification of rock types notably challenging. Within all rock types, including the prominently exposed massive gabbroic rocks.

There are cataclastic structures and mylonitic textures. These cataclastic textures are manifested as pseudo layers, characterized by fine-grained patterns, with thicknesses ranging from a few centimeters to several meters (Figure 3a,b). These textures share similarities in appearance with marl, greywacke, and sandstone. The presence of these cataclastic layers can lead to misconceptions, giving the impression that the observed rocks are exclusively sedimentary in nature.

Field observations revealed structures within both low-temperature brittle zones and a high-temperature ductile zone. These structures include mylonitic foliation featuring SL-tectonites, stretching lineations, rootless isoclinal folds, asymmetric mantled porphyroclasts, and boudinage structures (Figure 3c–i).

To provide a more coherent and easily comprehensible overview of the Bulfat Igneous Complex in Qaladezha area, we organized the complex into several distinct components: the Walash group, the Bulfat group, and the metamorphic rocks. The subsequent sections will concisely describe these separate divisions.

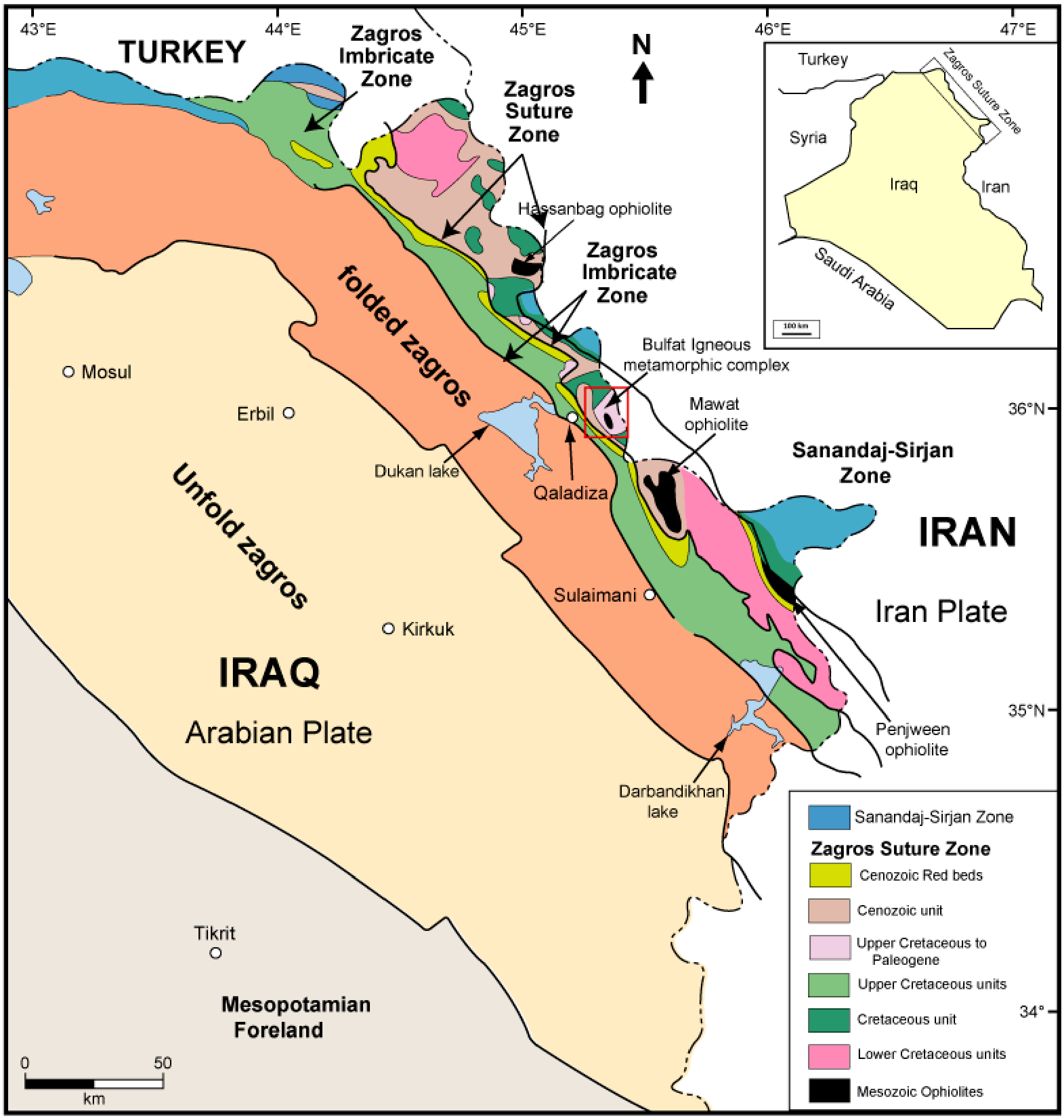

Figure 1. Regional tectonic map of northeastern Iraq showing the Zagros Suture Zone and the Mesozoic Neotethys ophiolite distribution after [14,23].

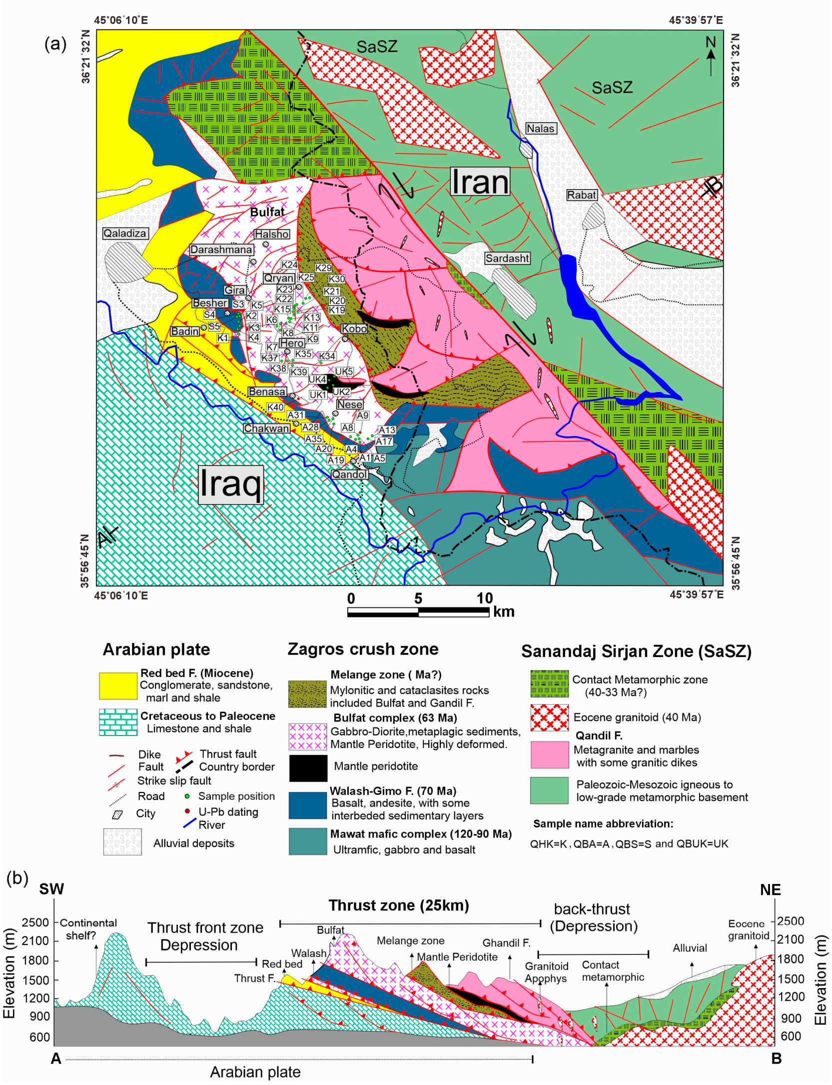

Figure 2. (**a**) Geologic map of the Bulfat Igneous Complex showing all geologic units and the names and locations of the study samples (**b**) (A,B) Geologic cross section of the Bulfat Igneous Complex.

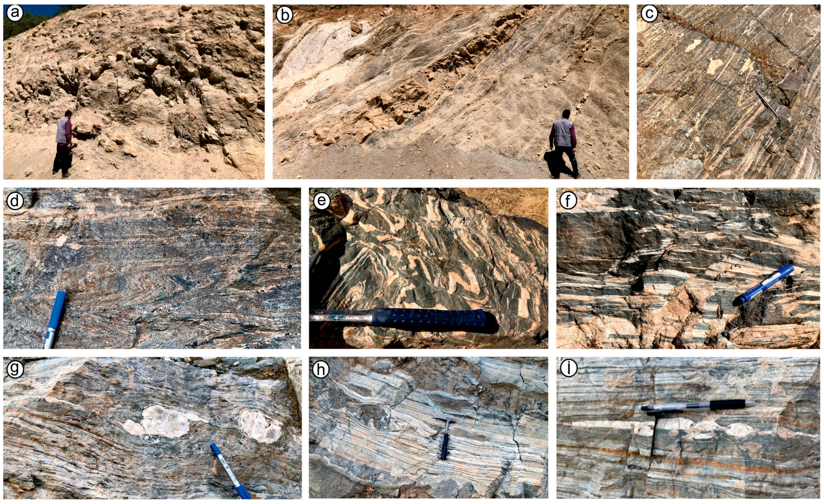

Figure 3. Field photographs showing deformational and structural features of the Bulfat Igneous Complex: (**a**,**b**) Cataclasitic structure and (**c**–**i**) mylonitic texture, stretching lineation, isoclinal folds, and boudinage structures (The structures indicate high-temperature ductile deformation).

2.1. Walash Group

The Walash group encompasses thick basaltic to andesitic rocks that stretch across the western limb of the Bulfat group. This group is characterized by the presence of pelagic red shale and serpentinite rocks (Figure 2a,b). The Walash group assumes a tadpole-like configuration and achieves its maximum thickness of about 2.5 km near Besher village in the northern section of the complex (Figure 2a). This geologic unit was initially identified by Buday [17] and is classified as Eocene rock formations within the Iraqi Zagros Suture Zone of Iraq. The Walash group has been extensively investigated by early studies [7,24,25]. Their research proposed that the group represents an island arc tectonic setting, featuring an intraoceanic system during the Eocene. This setting is comparable to the tectonic context of the Songhor–Baneh volcanic belt in western Iran [26]. The lower boundary of the Walash group is characterized by tectonic interactions with the Red Bed Series, evidenced by a highly deformed serpentinite horizon with thicknesses of 10–20 m. Meanwhile, the upper boundary remains indistinct with the Blufat group, owing to extensive deformation and thrusting.

2.2. Bulfat Group

The Bulfat group is poorly exposed lowland region and is composed of massive foliated gabbro intermingled withbasalt. This group, characterized by a rhombohedron shape, has been cut by strike-slip faults. Numerus duplicated structures feature repeated thrust faults has resulted in the thickening of the rock layers.

Peridotite mantle tectonitewith thicknesses of 500 to 1500 m, is prominently exposed around Pauza village, mainly along the southern and western edges of the Bulfat group (Figure 2a,b). These rocks are serpentinized and experienced considerable deformation during the obduction process. The presence of mantle peridotite can likely be attributed to obduction that occurred during the collision of the Arabian and Iranian tectonic plates.

2.3. Metamorphic Rocks

All rock units encompassing the Walash and Bulfat groups have undergone variable degree of metamorphism, spanning from the lower greenschist to the upper amphibolite-granulite facies. The degree of metamorphism progressively increases in the direction of the Zagros Suture Zone. This heightened metamorphism is notably conspicuous in the vicinity of Qandol village, positioned near the Iranian border and adjacent to ultramafic rocks. In this specific area, rocks distinctly display signs of high-grade metamorphism, characterized by evident stretching lineations, elongated hornblende, and feldspathic leucosomes (Figure 3d–i).

3. Petrography

3.1. Bulfat Group

The magmatic rocks within the Bulfat group can be divided into three main categories: ultramafic, mafic-dominated, and felsic rocks. These rocks are briefly described as follows:

Ultramafic rocks consist of mantle peridotite with a tectonite texture. They contain primary mineral phases including fine to medium olivine grains, coarse subhedral orthopyroxene, and anhedral oval-shaped chromite. Due to extensive serpentinization, alteration products such as serpentine, magnetite, and talc are present (Figure 4a). The mafic constituents found within the Bulfat group intrusion comprise gabbro, olivine gabbro, cumulate gabbro, and basalt. Gabbro, which holds a dominant presence among the rock types in the studied area, has a medium to coarse-grained textures and exhibits hypidiomorphic granular, cumulate, and ophitic textures (Figure 4b–e).

The primary magmatic mineral assemblage includes euhedral to subhedral plagioclase (30–70 vol.%), olivine (10–15 vol.%), and irregularly shaped clinopyroxene (10–20 vol.%), along with lesser amounts of K-feldspar and hornblende. Accessory minerals like ilmenite, magnetite, and titanite are also present. Amphibole, found in gabbroic rocks, often presents secondary minerals and forms a rim of coronitic reaction that contains pyroxene and olivine (Figure 4e). Basalts exhibit a range of textures including porphyritic, microlithic, spherulitic, and vesicular patterns. These rocks primarily comprise phenocrysts of plagioclase(20–50 vol.%) and clinopyroxene (5–15 vol.%), accompanied by smaller quantities of olivine, all within a fine-grained matrix distribution (Figure 4f,g).

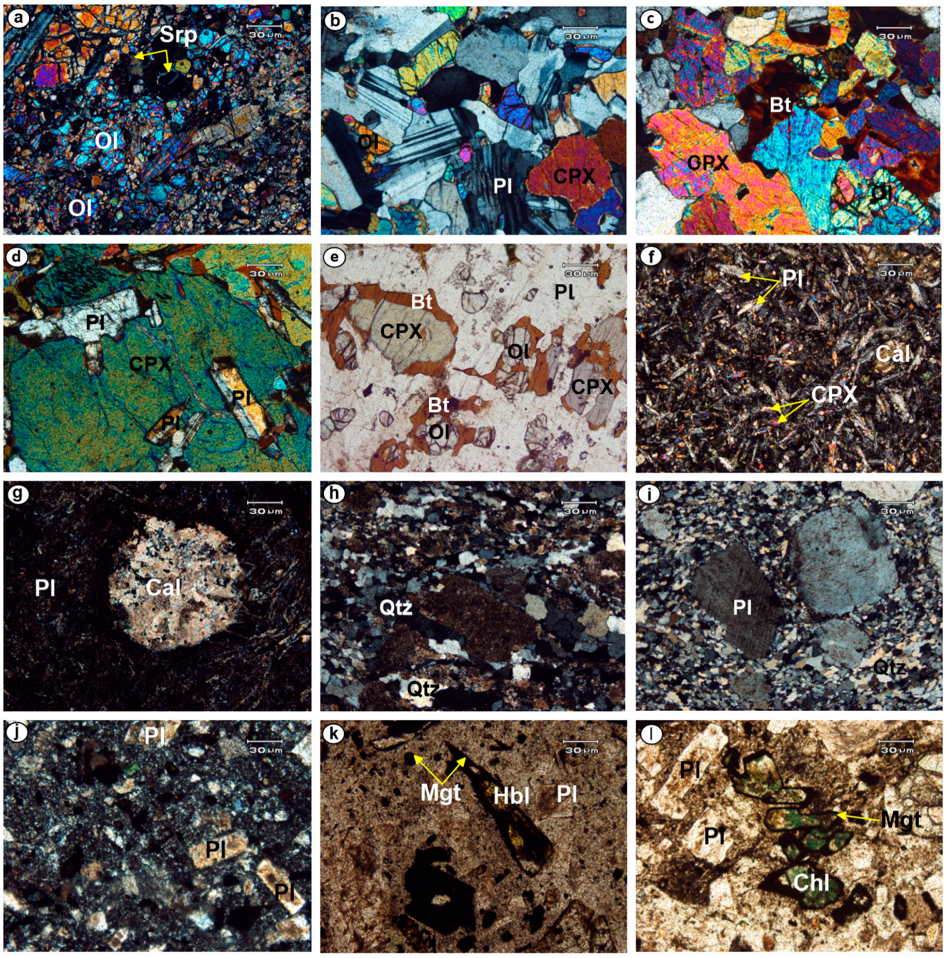

Figure 4. Photomicrographs of the Bulfat group (**a**–**i**) and Walash group (**j**–**l**) rocks: (**a**) Tectonite texture of mantle peridotite, (**b**,**c**) Coarse-grained gabbro with a hypidiomorphic granular texture, (**d**) Random plagioclase laths enclosed by pyroxene to provide an ophitic texture, (**e**) Olivine and pyroxene surrounded by coronitic biotite in gabbro, (**f**) Microlitic and porphyritic texture of basalt, (**g**) Vesicles filled with secondary calcite (**h**,**i**) Mylonitic texture of granitic rocks, plagioclase, and alkali feldspar porphyroclasts surrounded by quartz ribbons, (**j**) porphyritic and vitrophyric texture of andesite rocks with patchy zoning of plagioclase, and (**k**,**l**) Hornblende and chlorite in andesite rocks with a magnetite rim. Abbreviations: Cal = calcite, Chl = chlorite, Hbl = hornblende, Pl = plagioclase, CPx = clinopyroxene, Qtz = quartz, Ol = olivine, Srp = serpentine, Bt = Biotite, Mgt = magnetite. (Mineral abbreviations after [27]).

The felsic rocks is of a trondhjemite composition and have fine to coarse-grained textures; mylonitic texture is overprinted on these rocks. The main minerals present are plagioclase (60–80 vol.%), quartz (5–30 vol.%), and k-feldspar (0–10 vol.%) with minor mafic minerals, such as amphibole (2 vol.%). Other minerals present in the rocks include biotite, Fe–Ti oxides, apatite, monazite, and zircon (Figure 4h,i).

3.2. Walash group

The Walsh volcanic rocks are mostly basaltic andesites to andesite and have porphyritic, vitrophyric, and ophitic textures (Figure 4j–l). Primary minerals include plagioclase laths (20–50 vol.%) and clinopyroxene (5–15 vol.%). Altered plagioclase exhibits distinct irregular and oscillatory zoning patterns, and plagioclase phenocrysts commonly experience changes that result in the formation of secondary calcite and sericite.

4. Analytical Methods

Forty-six representative samples from the study region were precisely selected for comprehensive whole-rock analyses. These analyses encompass major, trace, and rare earth elements (REE) and were conducted at the ALS Laboratory Group in Spain, employing inductively coupled plasma mass spectrometry (ICP-MS).

The strontium (Sr) and neodymium (Nd) isotope ratios of the samples were measured at Nagoya University using the thermal ionization mass spectrometer (TIMS) GVI IsoProbe-T. The Sr-Nd isotope ratios were corrected based on $^{86}Sr/^{88}Sr$ (0.1194) $^{146}Nd/^{144}Nd$ (0.7219) for mass fractionation respectively. NIST-SRM987 and JNdi-1 were the natural Sr and Nd isotope ratio standards used in the study [28]. The measured values of $^{86}Sr/^{88}Sr$ and $^{143}Nd/^{144}Nd$ ratios were 0.71029 ± 0.00002 (SD, n = 9) and 0.51191 ± 0.00061 (SD, n = 3), respectively.

For the zircon U–Pb geochronology, two felsic samples from the Bulfat group and one andesitic sample from the Walash group were selected. about 1 kg of each sample was crushed, the minerals in the sample were separated using magnetic and heavy liquid bromoform, and using a binocular microscope, zircon grains in the samples were hand-picked for extraction from the heavy minerals. Zircon crystals placed in an epoxy resin were polished at the University of Sulaimani until the zircons could be seen clearly under reflected light. The zircons placed in the resin were observed at Nagoya University in Japan using a scanning electron microscope and their backscattered electron images were taken to determine their internal structure and cathodoluminescence (CL). The samples were dated at Nagoya University using inductively coupled plasma mass spectrometry (ICP-MS, Agilent 7700x) and NWR213 (Electro Scientific Industries, Portland, OR, USA) laser ablation system. The zircon age was determined using the 91500-zircon standard and NIST SRM 610 glass standard [29]. The measured ages of the 91500 and OD-3 zircon used in the study were 1058 ± 24 Ma (SD, n = 19) and 33.6 ± 2.0 Ma (SD, n = 13), respectively. The methods of U-Pb analysis is described in detail by [30,31]. The Concordia diagrams, histograms, and median ages were obtained using the ISOPLOT v.3.70 program [32].

5. Results

5.1. Zircon U–Pb Age

Two felsic samples from the Bulfat group were collected: one from the lighter-colored Trondhjemite leucosome part of a migmatite, visible as pale bands within the prevalent darker melanosome in the Qandol area (sample name QBA-9), and another from granite dyke that intrude into the gabbroic rocks in the Benasa area (sample name QHK-40). Additionally, a single sample (QBS-3) from the Walash group was chosen for the purpose of establishing the age of the zircon grains. The cathodoluminescence (CL) images of the three samples reveal that the zircon grains, ranging from 40 to 100 µm in length, appear colorless and transparent. Moreover, these grains have a euhedral to subhedral morphology. In most cases, the internal structure of a zircon grain exhibits oscillatory zoning patterns (Figure 5). The outcomes of the U–Pb dating are outlined in Supplementary Table S1. The thorium/uranium (Th/U) ratios of the zircon grains surpassed 0.2, indicating the magmatic origin of these zircons [33,34]. The Concordia ages of the samples QBA-9, QHK-40, and QBS-3 obtained using $^{206}Pb/^{238}U$ ratio are 63.7 ± 1.5 Ma (MSWD = 9.0, n = 20), 39.8 ± 0.91 (MSWD = 5.4, n = 21), and 69.7 ± 2.7 (MSWD = 2.7, n = 11), respectively (Figure 6a–i).

5.2. Whole Rock Chemistry

The results of whole rocks chemistry from the different types of rocks are presented in Supplementary Table S2 and we will discuss each group below:

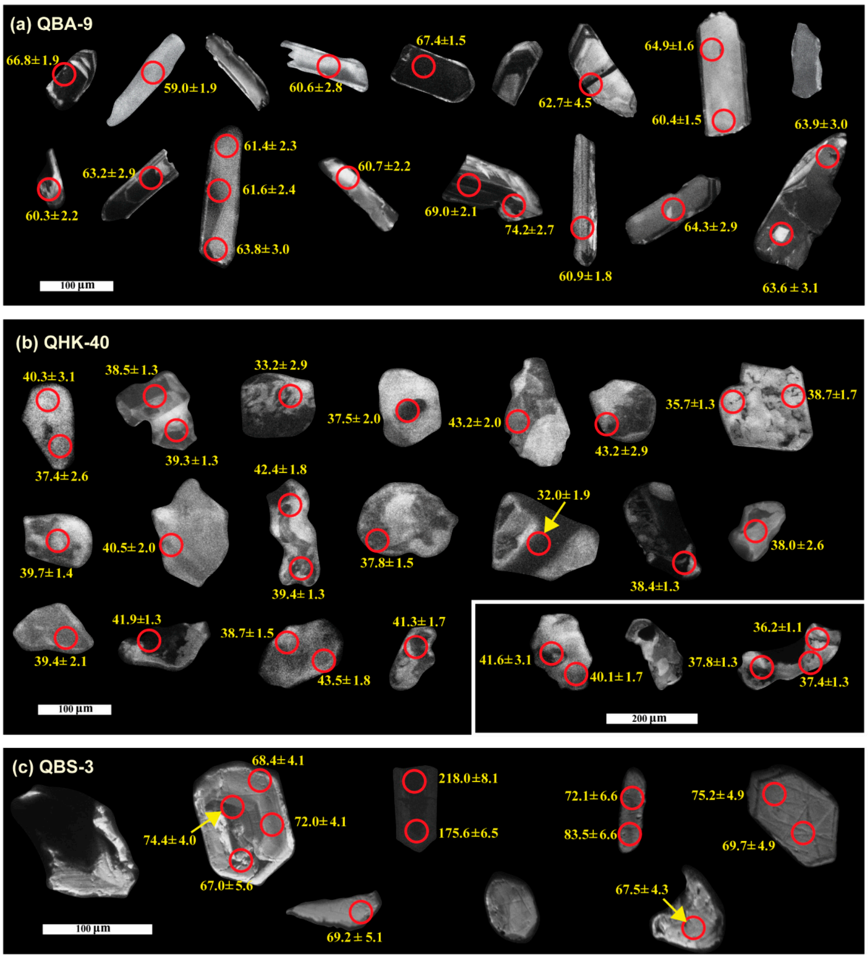

Figure 5. Cathodoluminescence images of zircon grains in (**a**) QBA-9 (**b**) QHK-40, and (**c**) QBS-3 samples (Red circles indicate the positions of the analytical spots, and yellow values represent ages at each point).

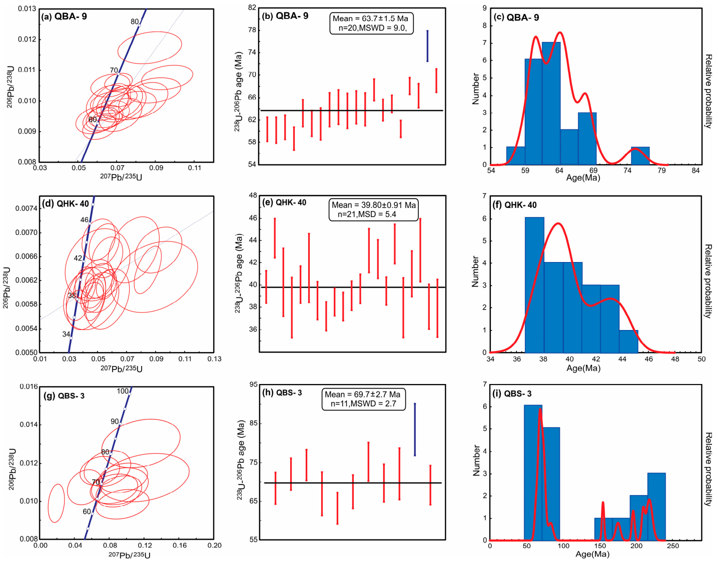

Figure 6. Concordia diagram, weighted mean ages, and histograms of zircon U–Pb. Geochronology of (**a**–**c**) QBA-9, (**d**–**f**) QHK-40, and (**g**–**i**) QBS-3 samples.

5.2.1. Ultramafic Rocks

The ultramafic rocks contain silicon dioxide (SiO_2; 38.3–39.4 wt.%); magnesium oxide (MgO; 43.2–44.3 wt.%); ferric oxide (Fe_2O_3; 7.96–8.84 wt.%); and small amounts (below 1 wt.%) of aluminum oxide (Al_2O_3), calcium oxide (CaO), and sodium oxide (Na_2O). In addition, they have abundant chromium (Cr; 2570–3040 ppm) and have a low total REE content of less than 2 ppm (Supplementary Table S2), aligning more closely with the characteristics of mantle tectonite dunite.

5.2.2. Mafic Rocks (Gabbro, Basalt, and Andesite)

Gabbro SiO_2 contents range from 41.8 to 52.4 wt.%, moderate amount of Na_2O (1.46–5.38 wt.%), and TiO_2 (0.06–2.84 wt.%), and varying concentrations of Al_2O_3 (7.53–25 wt.%), Fe_2O_3 (3.11–11.2 wt.%), CaO (8.49–23.3 wt.%), and MgO (3.29–9.38 wt.%). The Bulfat basalts display the following composition: SiO_2 content varies within a narrow range (50.4–53.1 wt.%); they contain high levels of Al_2O_3 (16.95–17.15 wt.%), Fe_2O_3 (7.95–9.09 wt.%), and a moderate amount of CaO (5.4–8.47 wt.%), TiO_2 (1.42–1.53 wt.%), and Na_2O (5.29–6.26 wt.%), along with MgO falling in the range of 3.43 to 3.89 (wt.%). Walash andesite has SiO_2 varying over a wide range (54.6–66.5 wt.%).

A high amount of Al_2O_3 (14.7–16.1 wt. %); and moderate amounts of Fe_2O_3 (3.34–5.29 wt.%), CaO (2.63–9.39 wt.%), Na_2O (3.36–6.92 wt.%), and MgO (1.88–6.12 wt.%).

In the Total Alkali versus Silica (TAS) classification diagram, all the mafic samples from Bulfat and Walash group are located within the gabbro, as well as the basalt and andesite fields respectively (Figure 7a,b). In the Alkali-FeO*-MgO (AFM) diagram (Figure 8a), the data points correspond to the gabbroic and basaltic rocks of the Bulfat group are positioned along the differentiation line that separates the tholeiitic and calc-alkaline series. Conversely, the data points represent Walash rocks are situated within the typical the calc-alkaline field (Figure 8a,c). The acidic rocks are primarily concentrated within the Trondhjemite field in the Orthoclase-Albite-Plagioclase diagram (Figure 8b).

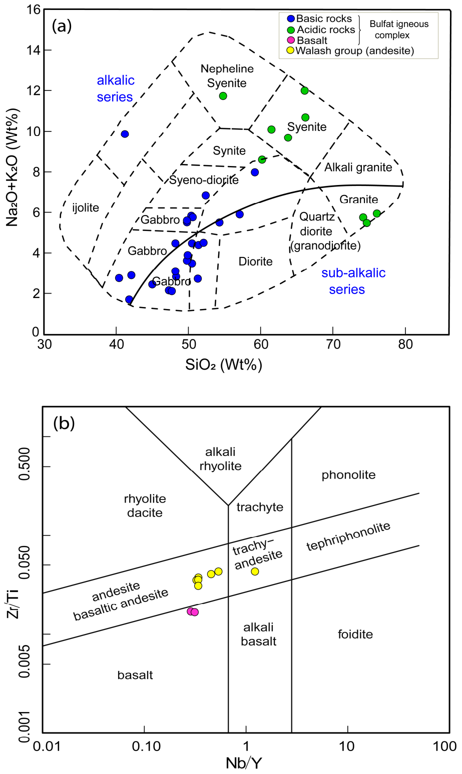

Figure 7. Whole rock chemical classification diagrams of the rocks present in the study area (**a**) Total alkali versus SiO_2 (TAS) diagram [35] and (**b**) Nb/Y versus Zr/diagram [36].

Gabbro exhibits notable negative anomalies of Rb, Nb, Th, Pr, and Ti, accompanied by moderate Ba, Nd, and Sr levels, along with significant positive anomalies of Pb (Figure 9a). These patterns differ from the primitive normalized patterns defined by [37].

Nevertheless, most of the gabbro samples, excluding the anorthosite sample (QHK-19) which exhibits a notably high $(La/Yb)_N$ value of 26.55, demonstrate a range of low to medium total rare earth element (REE) content, spanning from 6.24 to 226 ppm.

Moreover, these samples display fractionated patterns in terms of $(La/Yb)_N$ ratios, which vary between 0.71 and 10.48.

On the other hand, the basaltic rocks exhibit a subtle enrichment in elements such as K, Nb, and Zr (Figure 9c). The total Rare Earth Element (REE) content ranges from 67.85 to 76.72 ppm, and the pattern of fractionation, reflected in the $(La/Yb)_N$ ratio, falls within the range of 2.20 to 2.69.

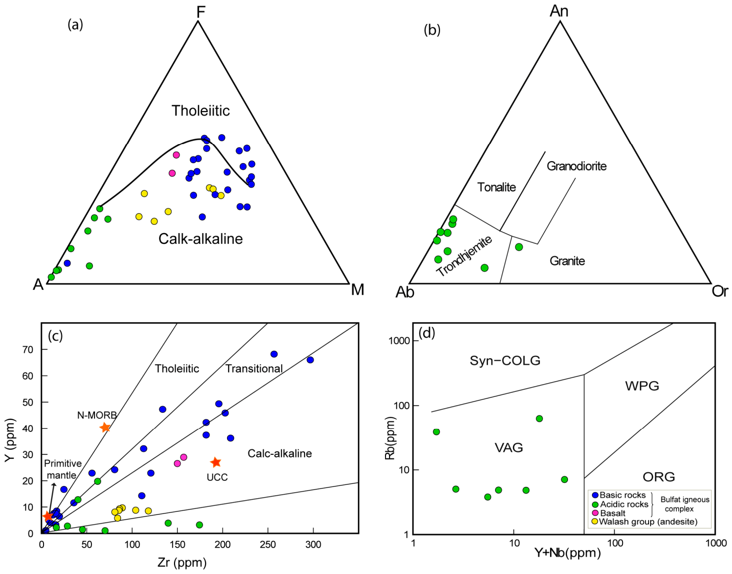

Figure 8. (**a**) AFM ternary diagram [38], (**b**) Normative An-Ab-Or classification diagram [39]. (**c**) Zr plotted vs. Y to reveal the magmatic affinity of rocks in the study area [40] and (**d**) Rb versus (Y + Nb) diagrams of acidic rocks [41].

The chondrite-normalized Rare Earth Element (REE) diagrams for gabbro consistently exhibit a flat trend, where the light REE are relatively enriched compared to the heavy REE. This pattern is accompanied by varying degrees of Eu anomalies, spanning from negative to notably positive values (ranging from 0.65 to 2.56) (Figure 9b).The chondrite-normalized pattern for Bulfat basalt demonstrates a flat profile akin to that of gabbro, with the exception of a notable europium (Eu) anomaly (Figure 9d).

Indeed, the Walash samples display an enrichment in light rare earth elements (LREE) rather than heavy rare earth elements (HREE), and they do not exhibit significant europium (Eu) anomalies (with Eu/Eu* ratios ranging from 0.99 to 1.14, as shown in Figure 8). Furthermore, the rocks characterized by high $(La/Yb)_N$ ratios (ranging from 5.90 to 16.51) also exhibit low contents of K and Pb (Figure 9c,d).

For better distinguishing tectonic settings and minimizing the potential effects of magma differentiation and contamination, only mafic to intermediate rocks were chosen for representation in the discrimination plotting diagrams. The Walash samples predominantly show characteristics associated with subduction zones due to their elevated Nb/Th ratios and substantial Th and La content. This alignment is consistently evident across multiple diagnostic diagrams, all of which consistently fall within the domain related to subduction arcs (Figure 10a–e). Meanwhile both gabbroic and basaltic members of the Bulfat group display characteristics indicative of extensional tectonic settings, such as continental rifts, back arc basins of mid-ocean ridge basalt (MORB), and ocean island basalt (OIB) domains

(Figure 10). In summary, the geochemical analyses affirm the presence of distinct differences between the Walash and Bulfat groups.

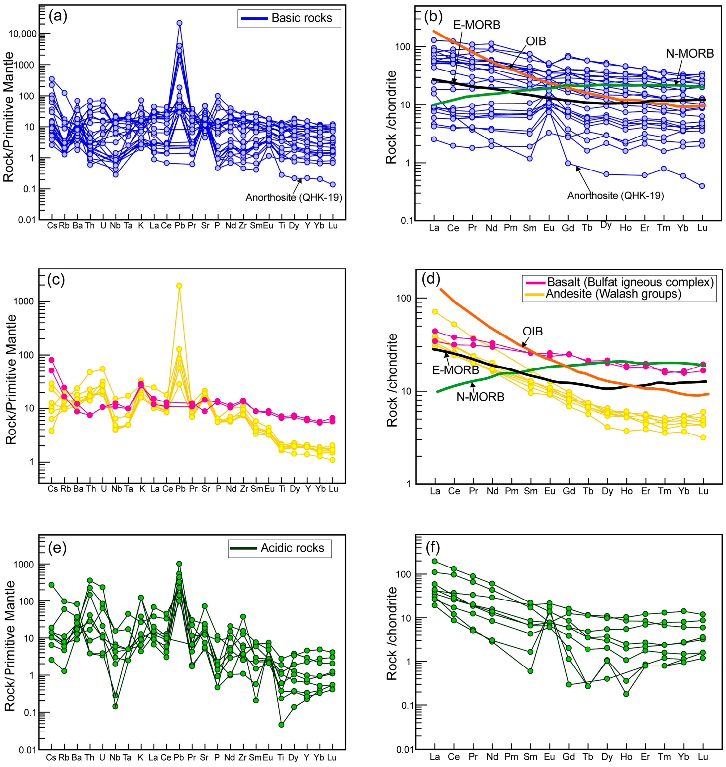

Figure 9. (**a**–**f**) Primitive mantle and chondrite-normalized diagrams [37] of the Bulfat and Walash Groups. (**b**,**d**) the mafic part compared with oceanic island basalt (OIB), enriched mid-ocean ridge basalt (E-MORB), and normal mid-ridge basalt (N-MORB) [34].

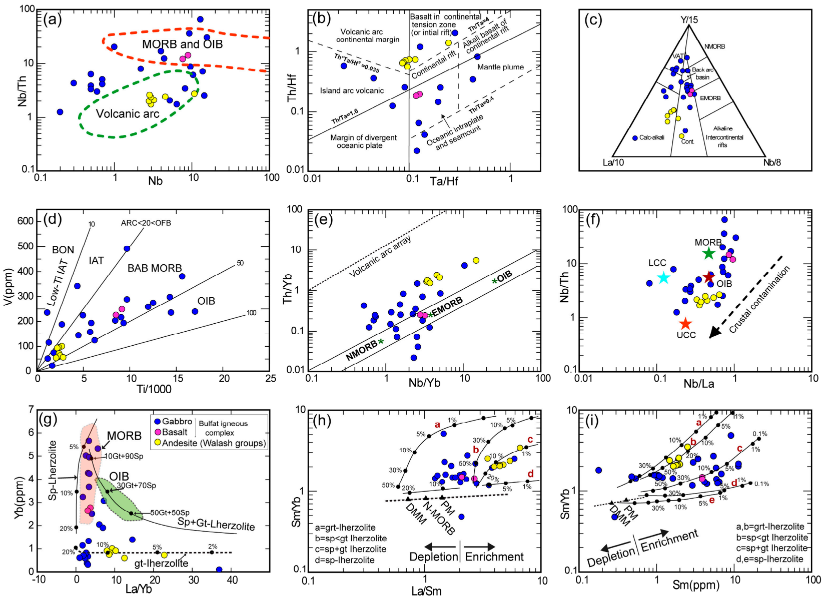

Figure 10. Discrimination and tectonic setting diagrams of the mafic samples: (**a**) Nb/Th versus Nb [42], (**b**) Ta/Hf versus Th/Hf ratios [43], (**c**) La/10–Y/15–Nb/8 [44] diagram, (**d**) V versus Ti [45] showing that most of the samples are in the back-arc basin, (**e**) Th/Yb versus Nb/Yb ratios [46], (**f**) Nb/La versus Nb/Th [47], (**g**–**i**) La/Yb versus Yb, La/Sm versus Sm/Yb, and Sm versus Sm/Yb ratios [48] demonstrating partial melting modeling with the melting degree indicated by the small black circle.

Discrepancies are evident in the La/Yb versus Yb, La/Sm versus Sm/Yb, and Sm versus Sm/Yb diagrams. Contrasts are observable in terms of the La/Yb, Sm/Yb, La/Sm, and Sm composition of the Walash and Bulfat specimens (Figure 10g–i). The Walash samples are primarily situated within the spinel-garnet lherzolite range (resulting from 5%–10% partial melting), whereas the Bulfat samples originate from a diverse source, displaying varied proportions of partial melting (ranging from 5% to 20%) in the spinel± garnet lherzolite. Consequently, the divergent geochemical attributes substantiate the distinctions between the Walash and Bulfat groups. To sum up, the geochemical data confirm significant distinctions between the Walash and Bulfat groups.

5.2.3. Felsic Rocks

The felsic rocks exhibit composition ranges that include SiO_2 (54.8–76.1 wt.%), Al_2O_3 (14.4–26.1 wt.%), and Fe_2O_3 (0.28–4.9 wt.%). Additionally, these rocks have a moderate CaO content (1.15–5.38 wt.%), remarkably low TiO_2 content (0.05–0.59 wt.%), elevated alkali content ($Na_2O + K_2O$ = 5.47–11.99 wt.%), and low K_2O content (0.13–3.66 wt.%). On the Or-An-Ab diagram (Figure 8b), they fall within the trondhjemite field. The variations observed in the major oxide compositions among the felsic rocks in the studied samples can generally be attributed to different tectonomagmatic processes that underlie the origin of the leucosome and feldspathic granite dikes within the Bulfat group [19,20].

In the primitive normalized trace element patterns, the felsic rocks exhibit distinct geochemical features, including positive anomalies in Th, Ba, and Sr, alongside negative anomalies in Rb, Sm, and Ti. Notably, they also show a prominent negative anomaly in Nb (Figure 9e). The total content of rare earth elements (REE) ranges from 13.64 to 170, and these samples are characterized by high fractionated patterns, with $(La/Yb)_N$ ratios spanning from 6.76 to 72. In the chondrite-normalized REE diagrams, the acidic sample displays enrichment in light rare earth elements (LREE) with relatively flat Heavy Rare Earth Elements (HREE) patterns (Figure 9f). With the exception of samples QHK-40 and QBA-28, all other samples have slightly positive Eu anomalies (Eu/Eu*) ratios ranging from 0.53 to 2. The granite tectonic discrimination diagram (Figure 8c) depicts all the rock samples situated within the volcanic arc field. these data provide further support for the presence of an arc-related tectonic environment for the Bulfat group.

5.3. Sr–Nd Isotope Ratios

Sr–Nd isotope ratios of the 17 Bulfat samples and those of the 4 Walash samples are presented in Supplementary Table S3. The initial Sr–Nd isotope ratios were calculated based on the zircon age of 63 Ma and 70 Ma, respectively. All of the Bulfat samples except the sample QHK-1 have a $^{87}Sr/^{86}Sr(i)$ ratio of 0.70320 to 0.70653, a $^{143}Nd/^{144}Nd(i)$ ratio in the range from 0.51267 to 0.512974, and positive εNd(t) values in the range from + 2.2 to +8.1. The sample QHK-1 has a negative εNd(t) of −2.5. The Walash samples have initial $^{87}Sr/^{86}Sr(i)$ values varying from 0.70371 to 0.70415, $^{143}Nd/^{144}Nd(i)$ varying from 0.51285 to 0.51289, and εNd(t) values varying from +5.9 to +6.8. In the εNd(t) versus $^{87}Sr/^{86}Sr(i)$ diagram (Figure 11a) [49], the Bulfat and Walash samples are plotted in the depleted mantle area close to the mantle array between OIB and MORB, and they would have been affected by seawater alteration. The scattering of the samples in the εNd(t) versus $^{87}Sr/^{86}Sr(i)$ diagram does not confirm the involvement of the continental crust component with the Bulfat and Walash rock sources. The SiO_2 versus $^{143}Nd/^{144}Nd(i)$ and $^{87}Sr/^{86}Sr(i)$ diagrams (Figure 11b,c) show an insignificant trend in the Bulfat and Walash samples indicating that the two groups were unaffected by wide mixing or differentiation.

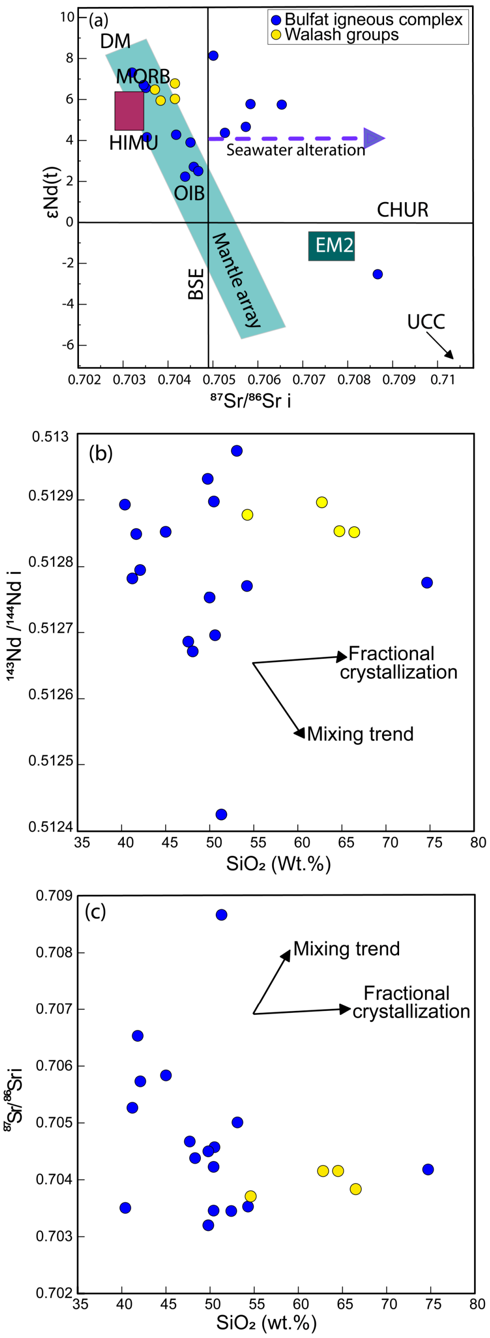

Figure 11. (**a**) Initial $^{87}Sr/^{86}Sr$ ratio versus εNd(t) of the Bulfat and Walash samples, showing their depleted mantle sources. The mantle component includes EM2 = enriched mantle, CHUR = chondritic uniform reservoir, and DM = depleted mantle [49], and (**b**,**c**) SiO_2 versus $^{87}Sr/^{86}Sr$ and $^{143}Nd/^{144}Nd$ plots, display the insignificant role of mixing or differentiation on the studied samples.

6. Discussions

6.1. Petrogenesis and Magma Sources

The isotope ratios and Rare Earth Element (REE) patterns of the Walash and Bulfat samples exhibit distinct differences, which can be summarized as follows:

The Walash samples display a negative trend in the REE pattern, characterized by a lower REE content in comparison to Ocean Island Basalt (OIB) and a higher Light Rare Earth Element (LREE) content relative to Normal Mid-Ocean Ridge Basalt (N-MORB) (Figure 9b,d). This alignment suggests compatibility with enriched Mid-Ocean Ridge Basalt (E-MORB). In contrast, the basaltic constituents of the Bulfat in addition to gabbroic samples demonstrate a relatively horizontal REE trend, closely resembling E-MORB, and they also exhibit some resemblance to both OIB and E-MORB patterns (Figure 9d). The presence of various REE patterns in the area suggests the potential occurrence of interactions between E-MORB-like and OIB melts, a scenario consistent with the involvement of both lithosphere and asthenosphere-derived melts within the Bulfat Igneous Complex.

The significantly positive εNd(t) values ranging from 6 to 7 suggest that the source magma for Walash andesite likely originated from a highly depleted mantle. Specifically, the εNd(t) values observed are consistent with those typically found beneath oceanic crust, which tends to exhibit higher εNd(t) values compared to the mantle beneath continental crust characterized by a lower level of depletion. Given the calc-alkaline nature of the Walash volcanic rocks (as seen in Figure 8a) and the elevated levels of mobile elements like Rb, Cs, La, and Pb, which are typically generated due to dehydration and alteration of the oceanic crust during subduction processes.

On the ^{87}Sr/^{86}Sr(i) versus εNd(t) diagram, the mafic samples from the Bulfat group can be categorized into three distinct clusters (Figure 11a). The two primary clusters are situated within the mantle array. The first cluster has εNd(t) values ranging from 6 to 8, while the second cluster exhibits lower ^{87}Sr/^{86}Sr(i) ratios within the range of 2 to 4. The third cluster stands out with a higher ^{87}Sr/^{86}Sr(i) ratio compared to the other two clusters. In the case of the third cluster, it's plausible that the elevated ^{87}Sr/^{86}Sr(i) ratios could be attributed to factors such as elevated Rb contents, potential losses of Rb–Sr during metamorphic alteration, and potential enrichment from fluids originating from the subducting slab during subduction processes.

The εNd(t) values of the Bulfat samples exhibit a range spanning from values characteristic of highly depleted mantle to those indicative of near-OIB-like and metasomatized mantle. This variability suggests that the Bulfat group likely originated from diverse sources. For instance, one potential source could involve a combination of less-altered mantle and newly depleted mantle that interacted with OIB-like melts. The wide spectrum of εNd values, coupled with tholeiitic to calc-alkaline affinity, along with the presence of various differentiated mafic constituents, leads us to propose the possibility of interactions between mantle melts from both the lithospheric and asthenospheric realms within a back-arc basin setting as another source scenario.

6.2. Geodynamic Implications

The Walash group was interpreted as an arc system with an age range of 43 to 24 Ma, situated within the Neotethys ocean, as proposed by Ali et al. [24]. This argument was based on ^{40}Ar–^{39}Ar dates obtained from single-grain or whole-rock analyses. It's important to note that the interpretation of ^{40}Ar–^{39}Ar date should take into account the potential complexities associated with the behavior of argon (Ar) during periods of high tectonic activity and deformation. These factors can influence the reliability and accuracy of age determinations in such geologic settings.

The currently available geochronological data for the Walash group primarily stem from ^{40}Ar–^{39}Ar step-heating analyses, as described in the works of [8,9,24]. Nonetheless, these dates are considered more indicative of metamorphic ages rather than magmatic ages. This interpretation is influenced by the fact that the gathered ^{40}Ar–^{39}Ar radiometric dating results, spanning various rock types within the ophiolite-dominated region of northwestern Zagros, Iraq, tend to converge around the timeframe of about 40 Ma [4]. This particular timing corresponds with the collision event between the Arabian and Eurasian tectonic plates. It is also corroborated by the presence of syn-collisional granites discovered in the Baneh area [50,51] and supported by additional sources [3].

Therefore, the derived ^{40}Ar–^{39}Ar dates should be approached with caution and not readily accepted as accurate representations of the rock ages. Conversely, the U-Pb age of zircon, determined as about 70 million years in this study, holds greater credibility and is more readily acceptable as the accurate age of the Walash group in the studied region.

Simultaneously, all the available geochronologic data related to the age of Bulfat group, which are concentrated around the range of 39 to 41 Ma [18], suggest ages associated with resetting rather than the ages of intrusion. Ali [7] utilized the U-Pb dating method for one zircon grain and suggested an age of roughly 39.0 ± 0.5 Ma for the Bulfat young gabbro intrusion. These dates are linked to a tectonic-thermal event that acquired during the collision between the Arabian and Iranian tectonic plates.

The confirmation of the older age of the Bulfat group is provided by the SHRIMP zircon U-Pb dating, which yielded a radiometric age of 48 Ma for trondhjemitic dikes. These dikes, as reported by Nutman et al. [19], intrude the gabbroic member of the Bulfat group. This further solidifies the understanding of the Bulfat group's age as being older than previously thought. Moreover, additional support for intrusion within the Bulfat group prior to 50 Ma is presented by Elias et al. [21].

Considering the disparities with previously reported dates, our recent study with zircon U-Pb dating has yielded three distinct age values: 70 million years for Walash, 63 million years for Bulfat, and 40 million years for syn-collisional granite. This span of ages suggests that the Walash volcanic rocks and Bulfat mafic rocks likely originated within the context of the well developed in an intraoceanic arc-back-arc tectonic regime in the Neotethys ocean. To considering our new dates and also whole rocks chemistry and Sr-Nd isotope ratios, we suggest a new tectonic model for evolution of the magmatic rocks for the NE Iraq in the Late Creteacous-Paleocene. Our model can explain gradually (1) the formation of a late Cretaceous arc at 70 million years ago (Walash Arc), (2) the subsequent splitting to form a Paleocene back-arc basin at 63 million years ago (Bulfat Mafic) due to the extensional regime in the back-arc, and finally (3) the collision with the Arabian plate at 40 million years ago Figure 12a–d). Notably, this age spectrum diminishes towards the Iranian side of the two colliding tectonic plates (e.g., [50–52]).

The Walash and Bulfat groups underwent the gradual development of an arc and back-arc setting within an oceanic system, yielding magmatic rocks spanning a spectrum from calc-alkaline to tholeiitic compositions (70–63 Ma). During the closure of the back-arc basin shortly after the generation, the subduction renewed beneath the Iran side after 60 Ma in Paleocene. The subduction of Bulfat immature oceanic crust beneath Iran was dragged to a depth of 40–50 km and metamorphosed under high-temperature, low to medium pressure conditions which we report as mafic migmatite in this research for the first time. Subsequently, the amalgamation of these arc and back-arc magmatic rock assemblages between the Arabian and Iranian plates took place around 40 Ma. Certainly, this collision is known as Arabian-Van-Northern Sanandaj Sirjan zone collision in northwest Iran.

Our model is consistent with the idea of a gap in arc magmatic activity in the northwestern Iran from 80 to, 50 million years ago. This period likely witnessed an extensional regime affecting NW Iran and parts of Turkey, attributed to the cessation of Neotethys subduction beneath Iran [50]. In addition, the present model can explain the magmatism evolution in the Iran sides and Eocene syncollision magmatic in the Zagros Suture Zone like Mariwan [51,53] and Baneh [50].

Our proposed model highlights the Cretaceous period as the predominant phase of magmatic activity on the Iraqi side. This suggests that both the Walash and Bulfat groups originated within an oceanic context and were subsequently thrust over the Arabian passive margin, and this tectonism likely occurring around 40 million years ago or potentially even earlier. This tectonic action resulted in their overlapping with the Cenozoic Red Bed Series (RBS) situated in the hinterland of intermountain basins. The obtained robust zircon U-Pb ages of the Walash and Bulfat groups reported in this study align remarkably well with the ~70 million years, ~60 million years, and ~40 million years age peaks of detrital zircon ages identified in the underlying RBS [22].

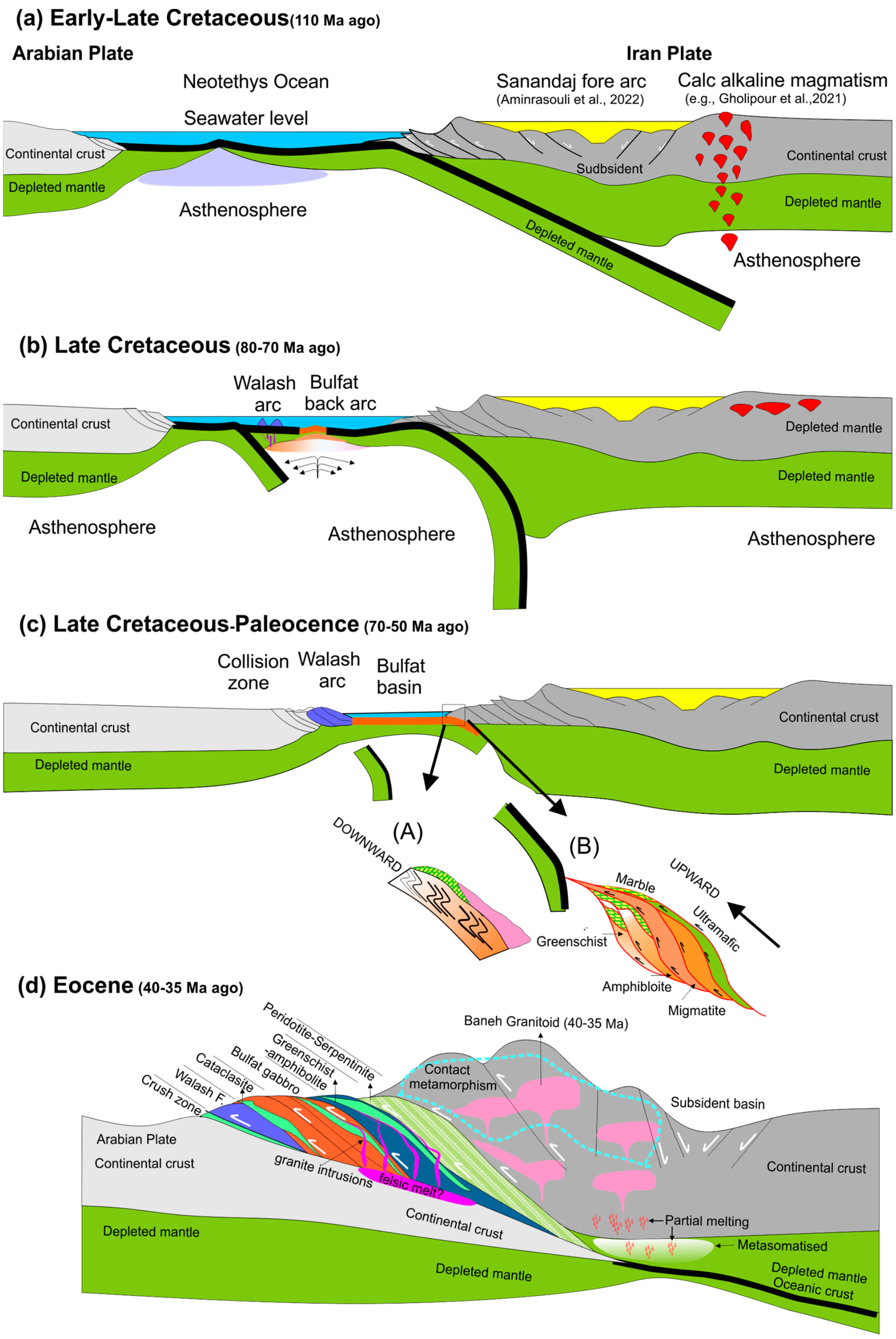

Figure 12. Schematic model showing: (**a**) subduction of the Neotethys ocean beneath Iran and development of the forearc basin [54], and typical arc magmatism on the Iranian side [55] present during the Early-late cretaceous, (**b**) Development of Walash and Bulfat arc and backarc systems in an intraoceanic system during the Cretaceous. (**c**) Soft collision of the Arabian plate with the Walash Group and cessation of Bulfat backarc development and initiation of hot and young backarc (immature oceanic crust) subduction beneath the Iranian plate and its metamorphosis into high-temperature and upper amphibolite facies (A) and scraped it (B) during the dragging of the oceanic crust to the depth in the Late Cretaceous-Paleocene, (**d**) Collision of the Arabian and Iranian plates during the Eocene (40–35 Ma ago) and squeezing of Walash and Bulfat Groups between the two large plates generating syntectonic granite, such as Baneh-Mariwan bodies [1,4,19,22,50,51,56,57].

7. Conclusions

This research reveals that, in the context of the Late Cretaceous to Paleocene arc-back arc system framework within the Neotethys Ocean in Northeastern Iraq, there is a spatial and temporal correlation between the Walash and Bulfat groups. The new age data from three distinct rock types in the Bulfat area reveals the presence of arc and back-arc systems in the Neotethys Ocean during a short interval around 10 million years from 70 to 60 million years ago. As the Arabian plate moved north and northeastward, these systems underwent destruction. The Bulfat hot back-arc segment was subsequently subducted beneath the Iranian plate, experiencing high-temperature conditions until the final collision around 40 Ma ago. Consequently, the Walsh and Bulfat rocks were sandwiched between the Arabian and Iranian plates post-collision. The both lateral and thrusting of the Zagros faults strongly affected these complex and dynamic deformation is overprinted on the rocks. Furthermore, we hypothesize the likelihood of a soft collision approximately 60 million years ago between the Arabian plate and the Walsh arc, resembling a continental-arc collision. Finally, our present results show the Late Cretaceous were the main times for magmatism not Cenozoic, despite of previously published work in the area.

Supplementary Materials: The following supporting information can be downloaded at: https://www.mdpi.com/article/10.3390/min13111367/s1. Table S1: Result of LA-ICP-MS data of zircon grains for the Bulfat group (QBA-9 and QHK-40 samples) and Walash group (QBS-3 sample). Table S2: Major, trace, and rare earth element concentrations of the Bulfat group Walash groups. Table S3: Sr-Nd isotope data for the Bulfat and the Walash groups. Refs. [58,59] are cited in Supplementary Materials.

Author Contributions: Y.M.: Conceptualization, Supervision, Writing—Reviewing and Editing; K.A.: Data curation, Resources, Writing—Original draft preparation, Software, Methodology. H.A.: Supervision, Resources, Funding acquisition, Writing—Reviewing and Editing. All authors have read and agreed to the published version of the manuscript.

Funding: This research received no external funding.

Data Availability Statement: Not applicable.

Acknowledgments: This work is a part of second author's Ph.D. thesis. Zircon U-Pb age dating and Sr–Nd isotope ratios were supported by Nagoya University, Japan. Special thanks to Y. Asahara and K.Yamamoto for their kind supports. This work was partly supported by Japan Society for promotion of Science (JSPS) KAKENH1 grant numbers 17H01171 and 18H05447. We thank N. Daneshavar for techniqual assistant for zircon separation. H. Azizi would like to thank the Institute of Space Earth Environmental research center (ISEE), and the Society for the Promotion of Science (JSPS) for their support as visiting and researcher fellow in 2022. The quality of the paper has been notably enhanced by the constructive feedback provided by three anonymous reviewers.

Conflicts of Interest: The authors declare no conflict of interest.

References

1. Mohammad, Y.O.; Cornell, D.H.; Qaradaghi, J.H.; Mohammad, F.O. Geochemistry and Ar–Ar Muscovite Ages of the Daraban Leucogranite, Mawat Ophiolite, Northeastern Iraq: Implications for Arabia–Eurasia Continental Collision. *J. Asian Earth Sci.* **2014**, *86*, 151–165. [CrossRef]
2. Aziz, N.R.H.; Aswad, K.J.A.; Koyi, H.A. Contrasting Settings of Serpentinite Bodies in the Northwestern Zagros Suture Zone, Kurdistan Region, Iraq. *Geol. Mag.* **2011**, *148*, 819–837. [CrossRef]
3. Mohammad, Y.O. Cumulate and Tectonite Dunite from Mawat Ophiolite, Kurdistan Region, Northeastern Iraq: Field Evidence and Mineral Chemical Constraints. *Iraqi Bull. Geol. Min.* **2020**, *16*, 15–33.
4. Mohammad, Y.O.; Cornell, D.H. U–Pb Zircon Geochronology of the Daraban Leucogranite, Mawat Ophiolite, Northeastern Iraq: A Record of the Subduction to Collision History for the Arabia–Eurasia Plates. *Isl. Arc* **2017**, *26*, e12188. [CrossRef]
5. Mohammad, Y.O.; Maekawa, H. Origin of Titanite in Metarodingite from the Zagros Thrust Zone, Iraq. *Am. Mineral.* **2008**, *93*, 1133–1141. [CrossRef]
6. Ali, S.A. Petrogenesis of Metabasalt Rocks in the Bulfat Complex, Kurdistan Region, Iraqi Zagros Suture Zone. *Kirkuk Univ. J. Sci. Stud.* **2015**, *10*, 242–252. [CrossRef]
7. Ali, S.A. 39 Ma U-Pb Zircon Age for the Shaki-Rash Gabbro in the Bulfat Igneous Complex, Kurdistan Region, Iraqi Zagros Suture Zone: Rifting of an Intra-Neotethys Cenozoic Arc. *Ofioliti* **2017**, *42*, 69–80.

8. Aswad, K.J.; Ali, S.A.; Sheraefy, R.M.A.; Nutman, A.P.; Buckman, S.; Jones, B.G.; Jourdan, F. 40Ar/39Ar Hornblende and Biotite Geochronology of the Bulfat Igneous Complex, Zagros Suture Zone, NE Iraq: New Insights on Complexities of Paleogene Arc Magmatism during Closure of the Neotethys Ocean. *Lithos* **2016**, *266*, 406–413. [CrossRef]
9. Aswad, K.J.; Sheraefy, R.M.A.; Ali, S.A. Pre-Collisional Intrusive Magmatism in the Bulfat Complex, Wadi Rashid, Qala Deza, NE Iraq: Geochemical and Mineralogical Constraints and Implications for Tectonic Evolution of Granitoid-Gabbro Suites. *Iraqi Natl. J. Earth Sci.* **2013**, *13*, 103–137.
10. Buda, G. Igneous Petrology of the Bulfat Area (North-East Iraqi Zagros Thrust Zone). *Acta Mineral. Petrogr.* **1993**, *34*, 21–39.
11. Buday, T.; Jassim, S. *The Regional Geology of Iraq, Vol. 2: Tectonism, Magmatism and Metamorphism*; GEOSURV: Baghdad, Iraq, 1987; 352p.
12. Jassim, S.Z.; Goff, J.C. *Geology of Iraq*; DOLIN, sro: Prague, Czech Republic, 2006.
13. Ali, S.A.; Buckman, S.; Aswad, K.; Jones, B.; Ismail, S.; Nutman, A. Recognition of Late Cretaceous Hasanbag Ophiolite-Arc Rocks in the Kurdistan Region of the Iraqi Zagros Suture Zone: A Missing Link in the Paleogeography of the Closing Neotethys Ocean. *Lithosphere* **2012**, *4*, 395–410. [CrossRef]
14. Mohammad, Y.; Kareem, H.; Anma, R. The Kuradawe Granitic Pegmatite from the Mawat Ophiolite, Northeastern Iraq: Anatomy, Mineralogy, Geochemistry, and Petrogenesis. *Can. Mineral.* **2016**, *54*, 989–1019. [CrossRef]
15. Azizi, H.; Hadi, A.; Asahara, Y.; Mohammad, Y. Geochemistry and Geodynamics of the Mawat Mafic Complex in the Zagros Suture Zone, Northeast Iraq. *Open Geosci.* **2013**, *5*, 523–537. [CrossRef]
16. Al-Hamed, S.; Aswad, K.; Aziz, N. Geochemistry and Petrogenesis of Dioritic-Gabbroic Pegmatites in the Bulfat Complex, Qala Diza, Northeastern Iraq. *Iraqi Natl. J. Earth Sci.* **2020**, *20*, 64–90. [CrossRef]
17. Buday, T. *The Regional Geology of Iraq, Vol 1: Stratigraphy and Paleogeography*; Publications of Geological Survey of Iraq: Baghdad, Iraq, 1980; 445p.
18. Karo, N.M.; Oberhänsli, R.; Aqrawi, A.M.; Elias, E.M.; Aswad, K.J.; Sudo, M. New 40Ar/39Ar Age Constraints on Cooling and Unroofing History of the Metamorphic Host Rocks (and Igneous Intrusion Associates) from the Bulfat Complex (Bulfat Area), NE-Iraq. *Arab. J. Geosci.* **2018**, *11*, 234. [CrossRef]
19. Nutman, A.; Ali, S.; Mohammad, Y.; Jones, B.G.; Zhang, Q. The Early Eocene (48 Ma) Qaladeza Trondhjemite Formed by Wet Partial Remelting of Mafic Crust in the Arc-Related Bulfat Igneous Complex (Kurdistan, Iraq): Constraints on the Timing of Neotethys Closure. *Arab. J. Geosci.* **2022**, *15*, 679. [CrossRef]
20. Zrary, M.M.; Aqrawi, A.M.; Elias, E.M. Petrogenesis and Tectonic Setting of Shakha Rash Granitoid, Bulfat Intrusive Complex, Northeastern Iraq. *Arab. J. Geosci.* **2022**, *15*, 1375. [CrossRef]
21. Elias, E.M.; Al-Jubory, Z.J.; Aqrawi, A.M. Metamorphic Evolution of the Bulfat Belt (NE-Iraq): Evidence from 40Ar/39Ar Age Spectrum Measurements. *Iraqi Geol. J.* **2022**, *55*, 1–11. [CrossRef]
22. Koshnaw, R.I.; Schlunegger, F.; Stockli, D.F. Detrital Zircon Provenance Record of the Zagros Mountain Building from the Neotethys Obduction to the Arabia–Eurasia Collision, NW Zagros Fold–Thrust Belt, Kurdistan Region of Iraq. *Solid Earth* **2021**, *12*, 2479–2501. [CrossRef]
23. Al-Kadhimi, J.M.A.; Sissakian, V.K.; Fattah, A.S.; Deikran, D.B. *Tectonic Map of Iraq, Scale 1: 1000 000*, 2nd ed.; GEOSURV: Baghdad, Iraq, 1996.
24. Ali, S.A.; Buckman, S.; Aswad, K.J.; Jones, B.G.; Ismail, S.A.; Nutman, A.P. The Tectonic Evolution of a Neo-Tethyan (Eocene–Oligocene) Island-arc (Walash and Naopurdan Groups) in the Kurdistan Region of the Northeast Iraqi Zagros Suture Zone. *Isl. Arc* **2013**, *22*, 104–125. [CrossRef]
25. Ali, S.A.; Aswad, K.J. SHRIMP U-Pb Dating of Zircon Inheritance in Walash Arc Volcanic Rocks (Paleogene Age), Zagros Suture Zone, NE Iraq: New Insights into Crustal Contributions to Trachytic Andesite Generation. *Iraqi NJ Earth Sci.* **2013**, *13*, 45–58.
26. Azizi, H.; Moinevaziri, H. Review of the Tectonic Setting of Cretaceous to Quaternary Volcanism in Northwestern Iran. *J. Geodyn.* **2009**, *47*, 167–179. [CrossRef]
27. Whitney, D.L.; Evans, B.W. Abbreviations for Names of Rock-Forming Minerals. *Am. Mineral.* **2010**, *95*, 185–187. [CrossRef]
28. Tanaka, T.; Togashi, S.; Kamioka, H.; Amakawa, H.; Kagami, H.; Hamamoto, T.; Yuhara, M.; Orihashi, Y.; Yoneda, S.; Shimizu, H. JNdi-1: A Neodymium Isotopic Reference in Consistency with LaJolla Neodymium. *Chem. Geol.* **2000**, *168*, 279–281. [CrossRef]
29. Goolaerts, A.; Mattielli, N.; De Jong, J.; Weis, D.; Scoates, J.S. Hf and Lu Isotopic Reference Values for the Zircon Standard 91500 by MC-ICP-MS. *Chem. Geol.* **2004**, *206*, 1–9. [CrossRef]
30. Kouchi, Y.; Obara, H.; Fujimoto, T.; Orihashi, Y.; Haruta, Y.; Yamamoto, K. Zircon U–Pb Dating by 213 Nm Nd. YAG Laser Ablation Inductively Coupled Plasma Mass Spectrometry. Optimization of the Analytical Condition to Use NIST SRM 610 for Pb/U Fractionation Correction. *Chikyu Kagaku* **2015**, *49*, 19–35.
31. Orihashi, Y.; Nakai, S.; Hirata, T. U-Pb Age Determination for Seven Standard Zircons Using Inductively Coupled Plasma–Mass Spectrometry Coupled with Frequency Quintupled Nd-YAG (Λ = 213 Nm) Laser Ablation System: Comparison with LA-ICP-MS Zircon Analyses with a NIST Glass Reference Material. *Resour. Geol.* **2008**, *58*, 101–123. [CrossRef]
32. Ludwig, K. *User's Manual for a Geochronological Toolkit for Microsoft Excel*; Special Publication Vol 4; Berkeley Geochronology Center: Berkeley, CA, USA, 2003.
33. Hoskin, P.; Black, L. Metamorphic Zircon Formation by Solid-state Recrystallization of Protolith Igneous Zircon. *J. Metamorph. Geol.* **2000**, *18*, 423–439. [CrossRef]
34. Pei, F.; Xu, W.; Yang, D.; Zhao, Q.; Liu, X.; Hu, Z. Zircon U-Pb Geochronology of Basement Metamorphic Rocks in the Songliao Basin. *Chin. Sci. Bull.* **2007**, *52*, 942–948. [CrossRef]

35. Cox, K.; Bell, J.; Pankhurst, R. *The Interpretation of Igneous Rocks*; George Allen: London, UK, 1979.
36. Pearce, J.A. A User's Guide to Basalt Discrimination Diagrams. In *Trace Element Geochemistry of Volcanic Rocks: Applications for Massive Sulphide Exploration*; Short Course Notes; Geological Association of Canada: St. John's, NL, Canada, 1996; Volume 12, p. 113.
37. Sun, S.-S.; McDonough, W.F. *Chemical and Isotopic Systematics of Oceanic Basalts: Implications for Mantle Composition and Processes*; Geological Society: London, UK, 1989; Volume 42, pp. 313–345.
38. Irvine, T.N.; Baragar, W. A Guide to the Chemical Classification of the Common Volcanic Rocks. *Can. J. Earth Sci.* **1971**, *8*, 523–548. [CrossRef]
39. O'conner, J. A Classification of Quartz-Rich Igneous Rocks Based on Feldspar Ratios. *US Geol. Surv. Prof. Pap.* **1965**, *525B*, 82.
40. MacLean, W.H.; Barrett, T.J. Lithogeochemical techniques using immobile elements. *J. Geochem. Explor.* **1993**, *48*, 109–133. [CrossRef]
41. Pearce, J.A.; Harris, N.B.; Tindle, A.G. Trace Element Discrimination Diagrams for the Tectonic Interpretation of Granitic Rocks. *J. Petrol.* **1984**, *25*, 956–983. [CrossRef]
42. Pearce, J.A. Immobile Element Fingerprinting of Ophiolites. *Elements* **2014**, *10*, 101–108. [CrossRef]
43. Yunliang, W.; Chengjiang, Z.; Shuzhi, X. Th/Hf-Ta/Hf Identification of Tectonic Setting of Basalts. *Acta Petrol. Sin.* **2001**, *17*, 413–421.
44. Cabanis, B.; Lecolle, M. Le Diagramme La/10-Y/15-Nb/8: Un Outil Pour La Discrimination Des Séries Volcaniques et La Mise En Évidence Des Processus de Mélange et/Ou de Contamination Crustale. *C. R. Acad. Sci. Sér. 2 Méc. Phys. Chim. Sci. Univers Sci. Terre* **1989**, *309*, 2023–2029.
45. Shervais, J.W. Ti-V Plots and the Petrogenesis of Modern and Ophiolitic Lavas. *Earth Planet. Sci. Lett.* **1982**, *59*, 101–118. [CrossRef]
46. Pearce, J.A. Geochemical Fingerprinting of Oceanic Basalts with Applications to Ophiolite Classification and the Search for Archean Oceanic Crust. *Lithos* **2008**, *100*, 14–48. [CrossRef]
47. Zhang, C.-L.; Zou, H.-B.; Yao, C.-Y.; Dong, Y.-G. Origin of Permian Gabbroic Intrusions in the Southern Margin of the Altai Orogenic Belt: A Possible Link to the Permian Tarim Mantle Plume? *Lithos* **2014**, *204*, 112–124. [CrossRef]
48. Aldanmaz, E.; Pearce, J.A.; Thirlwall, M.; Mitchell, J. Petrogenetic Evolution of Late Cenozoic, Post-Collision Volcanism in Western Anatolia, Turkey. *J. Volcanol. Geotherm. Res.* **2000**, *102*, 67–95. [CrossRef]
49. Zindler, A.; Hart, S. Chemical Geodynamics. *Annu. Rev. Earth Planet. Sci.* **1986**, *14*, 493–571. [CrossRef]
50. Azizi, H.; Hadad, S.; Stern, R.J.; Asahara, Y. Age, Geochemistry, and Emplacement of the ~40-Ma Baneh Granite–Appinite Complex in a Transpressional Tectonic Regime, Zagros Suture Zone, Northwest Iran. *Int. Geol. Rev.* **2019**, *61*, 195–223. [CrossRef]
51. Rezaei, F.; Azizi, H.; Asahara, Y. Tectonic Significance of the Late Eocene (Bartonian) Calc-Alkaline Granitoid Body in the Marivan Area, Zagros Suture Zone, Northwest Iran. *Int. Geol. Rev.* **2022**, *64*, 1081–1096. [CrossRef]
52. Azizi, H.; Tsuboi, M. The Van Microplate: A New Microcontinent at the Junction of Iran, Turkey, and Armenia. *Front. Earth Sci.* **2021**, *8*, 574385. [CrossRef]
53. Sepahi, A.A.; Shahbazi, H.; Siebel, W.; Ranin, A. Geochronology of Plutonic Rocks from the Sanandaj-Sirjan Zone, Iran and New Zircon and Titanite U-Th-Pb Ages for Granitoids from the Marivan Pluton. *Geochronometria* **2014**, *41*, 207–215. [CrossRef]
54. Amin-Rasouli, H.; Azizi, H.; Asahara, Y.; Armstrong-Altrin, J.S.; Mahmodyan, S. Whole-Rock Chemistry and Sr Isotope Concentrations in the Upper Cretaceous Shale, Western Iran: Evidence for a Transition from Trench to Fore-Arc Setting. *Arab. J. Geosci.* **2022**, *15*, 1513. [CrossRef]
55. Gholipour, S.; Azizi, H.; Masoudi, F.; Asahara, Y.; Tsuboi, M. Zircon U-Pb Ages, Geochemistry, and Sr-Nd Isotope Ratios for Early Cretaceous Magmatic Rocks, Southern Saqqez, Northwestern Iran. *Geochemistry* **2021**, *81*, 125687. [CrossRef]
56. Mohammad, Y.O.; Ali, S.A.; Aziz, N.R.; Yara, I.O.; Abdulla, K.L. Comment on "Generation and Exhumation of Granitoid Intrusions in the Penjween Ophiolite Complex, NW Zagros of the Kurdistan Region of Iraq: Implications for the Geodynamic Evolution of the Arabia-Eurasia Collision Zone" by Ismail et al., 2020, V. 376–377, 105714. *Lithos* **2021**, *390*, 105915.
57. Mohammad, Y.O.; Karim, K.H. Timing of the Arabia-Eurasia Continental Collision—Evidence from Detrital Zircon U-Pb Geochronology of the Red Bed Series Strata of the Northwest Zagros Hinterland, Kurdistan Region of Iraq: COMMENT. *Geology* **2019**, *47*, e471. [CrossRef]
58. Stacey, J.S.; Kramers, J.D. Approximation of Terrestrial Lead Isotope Evolution by a Two-Stage Model. *Earth Planet. Sci. Lett.* **1975**, *26*, 207–221. [CrossRef]
59. DePaolo, D.J.; Wasserburg, G. Nd Isotopic Variations and Petrogenetic Models. *Geophys. Res. Lett.* **1976**, *3*, 249–252. [CrossRef]